

Reducing the background temperature for cyclotron cooling in a cryogenic Penning–Malmberg trap

Cite as: Phys. Plasmas **29**, 083303 (2022); <https://doi.org/10.1063/5.0093360>

Submitted: 28 March 2022 • Accepted: 26 July 2022 • Published Online: 23 August 2022

 C. Amsler, H. Breuker,  S. Chesnevskaya, et al.



View Online



Export Citation



CrossMark

ARTICLES YOU MAY BE INTERESTED IN

[Positron generation via ultra-intense circularly polarized laser pulses colliding in near-critical-density plasmas with different thickness](#)

Physics of Plasmas **29**, 083103 (2022); <https://doi.org/10.1063/5.0104670>

[Resonance broadening effect for relativistic electron interaction with electromagnetic ion cyclotron waves](#)

Physics of Plasmas **29**, 082903 (2022); <https://doi.org/10.1063/5.0101792>

[High repetition rate mapping of the interaction between a laser plasma and magnetized background plasma via laser induced fluorescence](#)

Physics of Plasmas **29**, 082113 (2022); <https://doi.org/10.1063/5.0097748>

Submit Today!

Physics of Plasmas

Special Topic: Plasma Physics
of the Sun in Honor of Eugene Parker



AIP
Publishing

Reducing the background temperature for cyclotron cooling in a cryogenic Penning–Malmberg trap

Cite as: Phys. Plasmas **29**, 083303 (2022); doi: [10.1063/5.0093360](https://doi.org/10.1063/5.0093360)

Submitted: 28 March 2022 · Accepted: 26 July 2022 ·

Published Online: 23 August 2022




















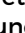



















View Online



Export Citation



CrossMark

C. Amsler,¹  H. Breuer,² S. Chesnevskaya,¹  G. Costantini,^{3,4}  R. Ferragut,^{5,6}  M. Giammarchi,⁶  A. Gligorova,¹  G. Gosta,^{3,4}  H. Higaki,⁷  E. D. Hunter,^{1,a)}  C. Killian,¹  V. Kletzl,¹  V. Kraxberger,¹  N. Kuroda,⁸  A. Lanz,^{1,9}  M. Leali,^{3,4}  V. Mäckel,¹  G. Maero,^{6,10}  C. Malbrunot,^{11,b)}  V. Mascagna,^{3,4}  Y. Matsuda,⁸  S. Migliorati,^{3,4}  D. J. Murtagh,¹  Y. Nagata,¹²  A. Nanda,^{1,9}  L. Nowak,^{9,11}  E. Pasino,^{6,10}  M. Romé,^{6,10}  M. C. Simon,¹  M. Tajima,¹³  V. Toso,^{5,6}  S. Ulmer,²  L. Venturelli,^{3,4}  A. Weiser,^{1,9}  E. Widmann,¹  T. Wolz,¹¹  Y. Yamazaki,²  and J. Zmeskal¹ 

AFFILIATIONS

¹Stefan Meyer Institute for Subatomic Physics, Austrian Academy of Sciences, 1030 Vienna, Austria

²Ulmer Fundamental Symmetries Laboratory, RIKEN, 351-0198 Saitama, Japan

³Dipartimento di Ingegneria dell'Informazione, Università degli Studi di Brescia, 25121 Brescia, Italy

⁴INFN sez. Pavia, 27100 Pavia, Italy

⁵L-NESS and Department of Physics, Politecnico di Milano, 22100 Como, Italy

⁶INFN sez. Milano, 20133 Milan, Italy

⁷Graduate School of Advanced Science and Engineering, Hiroshima University, 739-8530 Hiroshima, Japan

⁸Institute of Physics, Graduate School of Arts and Sciences, University of Tokyo, 153-8902 Tokyo, Japan

⁹Vienna Doctoral School in Physics, University of Vienna, 1090 Vienna, Austria

¹⁰Dipartimento di Fisica, Università degli Studi di Milano, 20133 Milan, Italy

¹¹Experimental Physics Department, CERN, 1211 Geneva, Switzerland

¹²Department of Physics, Tokyo University of Science, 162-8601 Tokyo, Japan

¹³RIKEN Nishina Center for Accelerator-Based Science, 351-0198 Saitama, Japan

^{a)}Author to whom correspondence should be addressed: eric.david.hunter@cern.ch

^{b)}Permanent address: TRIUMF, Vancouver, British Columbia V6T 2A3, Canada.

ABSTRACT

Magnetized nonneutral plasma composed of electrons or positrons couples to the local microwave environment via cyclotron radiation. The equilibrium plasma temperature depends on the microwave energy density near the cyclotron frequency. Fine copper meshes and cryogenic microwave absorbing material were used to lower the effective temperature of the radiation environment in ASACUSA's Cusp trap, resulting in significantly reduced plasma temperature.

© 2022 Author(s). All article content, except where otherwise noted, is licensed under a Creative Commons Attribution (CC BY) license (<http://creativecommons.org/licenses/by/4.0/>). <https://doi.org/10.1063/5.0093360>

I. INTRODUCTION

Antihydrogen, the simplest neutral system composed entirely of antimatter, has been produced by combining positron and antiproton plasmas in Penning traps^{1–3} at CERN's antiproton decelerator facility.⁴ Spectroscopy of the antiatom's microwave⁵ and optical⁶ transitions probes CPT invariance.⁷ Free-fall experiments^{8–10} will leverage the

neutrality of the anti-atom to directly test the applicability of the equivalence principle to antimatter. Such experiments may offer insight into the observed asymmetry between matter and antimatter in the universe.¹¹

The success of these experiments requires cooling the antimatter plasma to the lowest possible temperature.¹² For example, it is

assumed that the temperature of the antihydrogen produced during ALPHA's mixing protocol is close to the temperature of the positron plasma.¹² The positrons absorb both thermal energy from the antiprotons and binding energy from the nascent antihydrogen.¹³ Magnetized nonneutral plasma composed of electrons or positrons cools by emitting cyclotron radiation at frequencies close to $\omega_c/2\pi = 28 \text{ GHz} \times B[\text{T}]$. Cyclotron cooling usually proceeds according to Newton's law of cooling

$$dT/dt = -\Gamma(T - T_b) + H, \quad (1)$$

where the cooling rate $\Gamma = 0.26 \text{ s}^{-1} \times B[\text{T}]^2$ for electrons when two out of three dimensions radiate in the strong axial magnetic field. (The axial degree of freedom equilibrates with the transverse—radiating—degrees of freedom during electron–electron collisions.¹⁴ This equilibration time can be long for strongly magnetized electrons. For the coldest, lowest density plasma in this work, the time is of order 1 ms, which is still short compared with the cooling time Γ^{-1} .) The heating rate H , discussed below, has units of K s^{-1} . The plasma temperature T tends to the final temperature

$$T_f = T_b + H/\Gamma. \quad (2)$$

The temperature T_b is the hypothetical blackbody temperature, which best models the radiation environment at frequencies of interest to the plasma. It will be discussed in more detail below. The plasma heating rate H is often dominated either by the damping of plasma modes, which are excited by electrical noise on the electrodes, or by plasma expansion, which converts the potential energy of the concentrated charges into kinetic energy.¹⁵ Electrical noise at frequencies too low to excite a plasma mode may also contribute to plasma heating via non-adiabatic mixing between axial and transverse degrees of freedom when the plasma length changes.¹⁶

After a short time (typically 10 or 20 s), the plasma has passively cooled to $T \approx T_f$ and may be further cooled by evaporative cooling¹⁷ and adiabatic expansion.^{18,19} Such “active cooling” causes unavoidable expansion of the plasma and loss of particles. The total reduction in plasma temperature is typically a factor of 10 or less, depending on the initial temperature, the initial density, and how much loss is acceptable. The change in temperature is also temporary. The plasma quickly warms back up to its equilibrium temperature T_f . If active cooling is used to continuously suppress the plasma temperature below T_f (as in Ref. 12), then cyclotron radiation behaves as a heating rate proportional to the difference between T_f and the suppressed temperature. Thus, even where other cooling methods are considered, it is essential to minimize T_f and consequently both H and T_b .

The temperature T_b represents the microwave radiation environment, which couples to the cyclotron motion of the plasma. T_b is often assumed to be equal to the trap temperature T_t . However, that assumption is only valid when the microwaves produced by the plasma are efficiently absorbed by the trap electrodes, for example, when the electrodes form a microwave cavity.²⁰ When this is not the case, the value of T_b , and thus, the final temperature of the plasma T_f , becomes difficult to predict. The true value of T_b must involve an average of the temperatures of all possible absorbing surfaces, weighted by how resistive the surface is, how strongly the surface couples to a given microwave mode, and how strongly that mode couples to the collective modes of the plasma in a given geometry.²¹ In general, T_b is higher than T_t . The discrepancy will likely be greater for traps having fewer

absorptive surfaces in the cryogenic region and more solid angle open to room-temperature surfaces.

These ideas were explored in a preliminary way in Ref. 22 using a trap with a movable radiation shield (referred to in what follows as “trap II”). The data obtained suggested that the anomalously high final plasma temperature observed in the ASACUSA Cusp trap might be caused by microwaves leaking in from non-cryogenic regions. The present work compares that data with experiments in an older trap (“trap I”) and in a completely new setup designed to minimize T_b (“trap III”).

In this article, it is shown for the first time that restricting microwave propagation to the cryogenic region can lead to a dramatic reduction in plasma temperature. In each iterative trap upgrade, the radiation environment was intentionally modified and the base plasma temperature, which is taken as an index for T_b , was recorded in many experimental realizations (e.g., by varying plasma parameters, magnetic field, trap temperature, or trap pressure). All of the observations support the central hypothesis that T_b can be lowered by confining microwaves to the cryogenic part of the trap.

Section II introduces the apparatus, with emphasis on the successive modifications to the microwave environment and the accompanying changes in final plasma temperature. The representative plasma temperatures given in Sec. II are placed in context in Sec. III, where the dependence of plasma temperature on number of electrons N is given for each configuration of the experiment. This section also presents scans over trap temperature T_t and magnetic field B , which validate the cooling model presented above and illustrate the connection between T_f , T_b , and T_t . Section IV details the remaining differences between the configurations, which were not mentioned earlier because they do not affect microwave impedance. It is shown that most of these differences cannot contribute to the effect reported here. For the few details that could affect the plasma temperature, the most plausible mechanism is once again a small change in T_b , so the argument given above is unchanged. This view is further strengthened via comparisons with other Penning traps where charged particles have been cooled to cryogenic temperature. Section V is the conclusion.

II. TRAP GEOMETRY

The plasma studied in this work was confined near the center of the upstream magnetic mirror of ASACUSA's Cusp trap.²³ As shown in Fig. 1, the magnetic field may vary by 10% or more over the length of the plasma. By contrast, an ideal Penning–Malmberg trap would have a perfectly homogeneous magnetic field. In spite of this discrepancy, the plasma behavior relevant to the present work is essentially the same as in a standard trap. The plasma can be compressed with the standard rotating wall technique.²⁴ The plasma cools at the expected rate following Eq. (1) (see Sec. III). Expansion rates are similar to those of typical high-field Penning–Malmberg traps (i.e., 1000 s or more for the plasma radius to double),²² and the diocotron instability is sometimes present but rarely pronounced. Thus, the phenomena reported below are considered to be of general relevance to plasma cooling in Penning–Malmberg traps.

Figure 1 also shows how the microwave radiation background was modified in traps I–III. The primary method was to remove or replace the attenuating or reflecting structures at the openings of the trap (A1 and A2 in Fig. 1). The other method was to change the position of a movable radiation shield, which could be opened up to 90° as

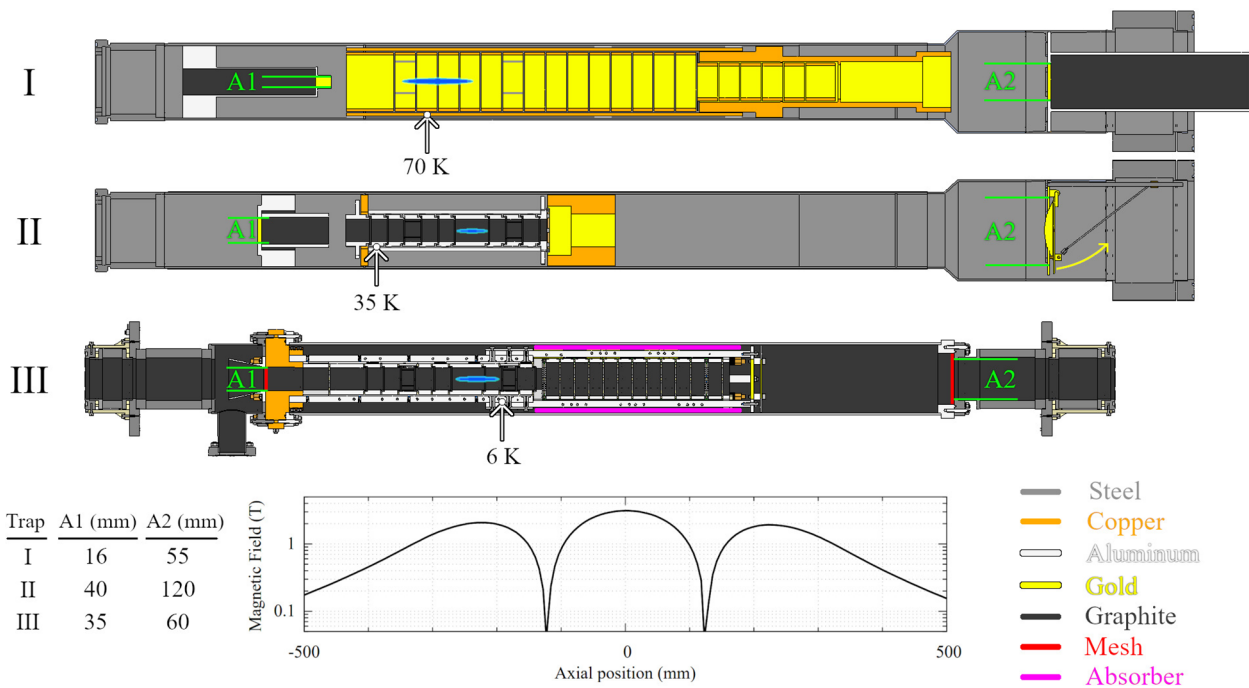


FIG. 1. Sketch of the traps and cusp magnetic field. Left is upstream, and right is downstream. Some aluminum structures have been omitted for clarity; these do not intercept the paths of microwaves going out of the trap. Materials having an influence on cryogenics or microwave propagation have been color coded as indicated in the key. The bright blue ellipses float at the approximate position of the plasma. The table at the bottom left gives the diameters of the apertures A1 and A2, which define the solid angle, with respect to the plasma, occupied by non-cryogenic surfaces. Vertical white arrows terminate on the sensors, which define the trap temperature T_t (see the Appendix B for more details).

indicated by the yellow arrow on the right side of trap II in Fig. 1. The shield was made of copper and electroplated with gold.

Trap III was designed specifically to prevent the plasma from coupling to regions outside the trap. For trap III, A1 and A2 were covered with a fine copper mesh (wire diameter 0.03, pitch 0.25 mm) sprayed with an alcohol-based colloidal graphite anti-static solution. Sprayed samples were inspected under a microscope to ensure that the spraying procedure did not reduce the transparency of the mesh (see the Appendix D). Theoretically,²⁵ such a mesh reduces transmitted microwave power at frequencies below 60 GHz (the cyclotron frequency at the highest magnetic field in the trap) by at least 20 dB. Trap III also contained long sections of resistively coated ceramic rod (“absorber” in Fig. 1), which had previously been employed for absorbing microwaves in accelerator beamlines by CERN’s RF group.²⁶ These sections were tied to the high-purity (5N) aluminum bars used for cooling the electrodes and protected from line-of-sight (infrared) radiation from outside.

Table I summarizes how the changes in trap geometry affected the amount of non-cryogenic surface seen by the plasma (expressed as relative solid angle) and the lowest achievable final plasma temperature T_f for a plasma containing $N = 2-3 \times 10^6$ electrons.

Plasma temperature measurements will be treated in more detail in Sec. III. However, the most significant trends may already be inferred from the data in Table I. Increasing the solid angle to surfaces outside the trap (trap I \rightarrow trap II) raised the base plasma temperature, and reducing the solid angle (trap II \rightarrow trap II a) reduced the

temperature. Likewise, closing the movable shield reduced both solid angle and plasma temperature. Reducing the trap temperature from 74 to 35 K (trap I \rightarrow trap II) was not correlated with any significant change in plasma temperature, while the reduction from 35 to 6 K (trap II \rightarrow trap III) was correlated with the most dramatic reduction in plasma temperature. The latter correlation seems to be a

TABLE I. Summary of the major differences affecting the radiation environment for traps I–III. The final plasma temperature T_f for $N = 2-3 \times 10^6$ is also given for each configuration (the trap II data appear also in Ref. 22). The solid angle seen by the plasma for surfaces external to the cryogenic trap is approximately $\Omega = \frac{\pi}{4}(A1/R1)^2 + \frac{\pi}{4}(A2/R2)^2$, where the apertures at distances R1 and R2 have diameter A1 and A2 (see Fig. 1). Trap II is the version shown in Fig. 1, while for trap II a, the diameter A1 was reduced by a factor of two (see also Appendix B). “Shield” refers to the state of the movable radiation shield (for traps II and II a). Considering only microwave propagation, Ω should be close to 0 in trap III because the apertures are covered by meshes.

Trap	$\Omega/4\pi$ (10^{-4})	Shield	T_t (K)	T_f (K)
I	11	...	74	130
II	20	Open	35	170
II	11	Closed	35	150
II a	12	Open	33	130
II a	3	Closed	33	110
III	11 (or 0)	...	6	25

coincidence; plasma temperature was still by far the lowest in trap III even when the trap was warmed to 60 K, as will be described in Sec. III.

III. PLASMA TEMPERATURE

The plasma temperature was measured by slowly releasing the charges onto a microchannel plate (followed by a phosphor screen) and correlating the time-dependent plasma current—measured by a silicon photomultiplier via the light emitted from the phosphor screen²⁷—with the time-dependent confinement potential in the trap.²⁸ Knowing the fraction of particles, which can escape as a function of confinement potential, one can reconstruct the high-energy tail of the Maxwell–Boltzmann distribution for the plasma. The temperature is then estimated by fitting the tail of the distribution to the form

$$A(t) = A_0 \exp[-U(t)/k_B T], \quad (3)$$

where $A(t)$ is proportional to the plasma current and $U(t)$ is the energy of the escaping charge with respect to the bottom of the confining well. $U(t)$ decreases as the well is opened on the upstream side. The diagnostic is straightforward to perform. However, the results are subject to a number of systematic errors, which are difficult to model. The systematic uncertainty associated with adiabatic effects (changes in plasma length during the diagnostic) often exceeds the statistical uncertainty obtained from imperfect cycle-to-cycle reproducibility. Fortunately, the effect of lowering T_b was observed to be largely independent of the correction factors assumed for the temperature (see the Appendix A). In this section, the plasma temperature is reported without attempting to correct for these systematic errors. Where error bars are given for a point, they represent the standard deviation for 4–6 nominally identical cycles.

Subsections III A–III D present four experiments, which alternately validate the central hypothesis of this article or show that it is robust across a wide range of plasma parameters. The heading of each subsection refers to the independent variable of the experiment.

A. Number of electrons

Figure 2 shows the final plasma temperature T_f obtained for a range of values of N , the number of electrons in the plasma. The plasma temperature is reported for four different trap configurations, corresponding to traps I, II (movable shield open and closed), and III in Table I. The range of plasma length, radius, and density for each data set is given in Appendix A.

For all values of N , the final plasma temperature was lowest for trap III, in which $3 < N < 35 \times 10^6$ electrons were cooled to $T_f \approx 25$ K. This was the only trap in which the plasma temperature came within 20 K of wall temperature. The black, red, and blue data sets in Fig. 2 correspond to progressively higher plasma temperature and more unscreened aperture looking out of the trap (Ω in Table I, noting that for trap III, Ω should be 0 when the meshes are taken into account). This correlation is monotonic in Fig. 2, in spite of the reversal in trap temperature (trap II was colder than trap I). In this sense, the data in Fig. 2 demonstrate the robustness of the conclusions drawn from Table I over a broad range of plasma parameters.

For trap II, the open squares (which correspond to the movable shield being open) are consistently 20 K higher than the filled squares. Experiments with the plasma held in different parts of the trap (reported in Ref. 22), where the cooling rate and final temperature were in general different, consistently reproduced this approximately

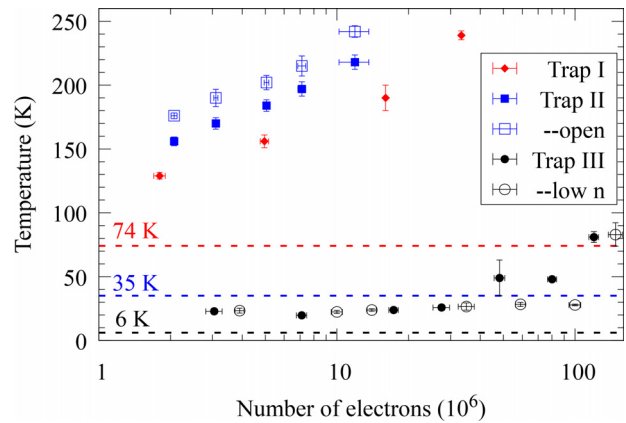


FIG. 2. Measured final temperatures for plasma with variable number of electrons N . Dashed lines indicate the temperature of the electrodes for each trap version. For trap II, the open square points correspond to the downstream thermal shield being open (the trap II data appear also in Ref. 22). For trap III, the open circles refer to a plasma preparation yielding a relatively low density than for the filled circles.

20 K offset when the shield was open. In every case where a comparison has been made, the sole effect of opening the shield was to increase T_b by about 20 K.

For traps I and II, T_f increases with N , whereas for trap III, this behavior is only apparent at high N . For trap I, a rotating wall was employed prior to cooling in order to keep the density high ($n > 5 \times 10^8 \text{ cm}^{-3}$) for all values of N , while for traps II and III, the cutting method was employed to reduce N without significantly altering the radius of the plasma. N was reduced by stretching the plasma axially and then cutting off a portion and discarding it. This procedure has the side effect of reducing the plasma density, which was relatively low even for the highest N points for trap III. Thus, the relative flatness of most of the trap III data set may be the result of a lower overall plasma density. This effect is a coincidence of the plasma parameters chosen and does not affect the main conclusion, as will be shown in Sec. III B.

B. Trap temperature

The background temperature T_b [see Eq. (2)] should be close to the temperature of the trap electrodes T_e when the plasma is not able to couple to surfaces outside the cryogenic region. In this situation, increasing or decreasing the electrode temperature should cause a proportionate increase or decrease in the final plasma temperature.

The most intuitive test of these ideas is to measure the plasma temperature as the trap is cooled down. Technically, it is not the simplest experiment, because traps that are designed to be cryogenic tend to have poor vacuum at room temperature. It was found that trap III could be run normally once the temperature had fallen to about 200 K. Starting at this point and continuing until the trap reached its base temperature, plasma was repeatedly prepared and diagnosed after 20 s of cooling. The results are shown in Fig. 3. While T_f does qualitatively track the changes in T_b , the correspondence is not exact. The gap between the two curves gets smaller over time, beginning with $\Delta T \approx 65$ K and settling ultimately to $\Delta T \approx 32$ K. In the absence of

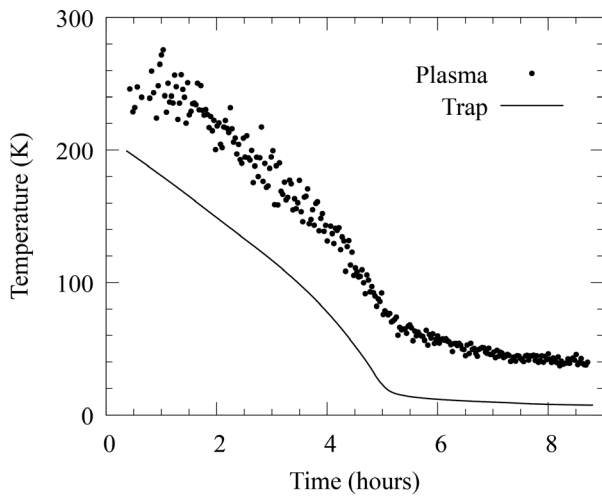


FIG. 3. Relation between final plasma temperature and the temperature of trap III as the trap was cooled down from room temperature by both coldheads working simultaneously. As the trap cooled, the plasma temperature fell, maintaining an offset of about 60 K for the first four hours. At later times, the offset was smaller, suggesting that the plasma was coupling to surfaces, which did not cool as quickly as the temperature sensor. The temperatures finally stabilized ($t > 20$ h) at 38 ± 3 K for the plasma and 6.0 K for the trap. The plasma parameters for this data set were fixed at $N = 15.1 \times 10^6$, $n = 1.1 \times 10^9 \text{ cm}^{-3}$, $r_p = 0.39 \text{ mm}$, $L_p = 3.6 \text{ cm}$.

vacuum effects (see below), this is an indication that T_b was set partly by an object, which cooled down more slowly than T_t . It is therefore likely that $T_b > T_t$.

The plasma used for this experiment was prepared using the SDREVC technique.²⁹ The three directly measurable quantities (space charge, plasma radius, and number of electrons) varied within a range smaller than 2% from the start to the end of the scan. A small plasma radius (and high density) was chosen to compensate for a bias in the data presented in Sec. III A. For the data in Fig. 2, the density of the plasma in trap III was systematically low, and the radius systematically high, compared to the parameters for the tests in traps I and II (see the Appendix A). The incommensurate ranges chosen for these plasma parameters made it impossible to conclude that the discrepancy in final plasma temperature was due to the microwave environment alone. Some or all of the difference in temperature could be due to the different plasma density and radius. To check that, the trap III data shown in Fig. 3 were taken with a plasma having higher density and slightly lower radius than the trap II plasma in Fig. 2. In trap III, the temperature of the high-density plasma approached a limit $T_f \approx 40$ K, which is more than 100 K lower than what could be achieved in traps I and II. While the final temperature in Fig. 3 is slightly higher than for the lower-density trap III data in Fig. 2, this is a small effect compared with the difference between the traps.

C. Trap pressure

As the trap cools, residual gas freezes onto the walls of the vacuum chamber and the pressure decreases. This vacuum effect could potentially account for the decreasing offset between the two curves in Fig. 3. One might even argue in general that the low temperatures obtained in trap III could be due to the removal of hydrogen, which

only freezes out for $T_t < 10$ K. The vacuum quality could affect the plasma temperature. For example, at sufficiently high pressure, the plasma expands more quickly due to collisions with neutrals. More plasma expansion would lead to a higher temperature via expansion heating (see Sec. I). However, in the 1–2 T field of the Cusp, the expansion due to collisions with neutrals is too small to provide significant heating, providing that the pressure is well below 10^{-8} mbar (at room temperature).³⁰ Moreover, the expansion rate in trap II was extremely low—the plasma took thousands of seconds to double in radius. Moreover, there could be more exotic effects such as heating due to a “wind” of 300 K molecules streaming down the pipe. In an attempt to rule out any such vacuum effect, the pressure in the trap was increased by allowing the entire cold bore to warm up.

Figure 4 shows the time evolution of typical plasma temperature as the temperature of trap III was varied by turning the two coldheads on and off. The upstream (US) coldhead was directly connected to the bars, which cool the electrodes, and therefore had a more rapid effect on the measured trap temperature than the downstream (DS) coldhead. As the trap warmed up, gases frozen onto cryogenic surfaces in the trap were liberated and increased the measured pressure. The pressure was measured in a room temperature region external to the trap. When the trap is also at room temperature, this pressure is typically below 10^{-8} mbar. During periods of strong off-gassing, the pressure rose well above this room-temperature value, implying that the trap was releasing more gas than was being cryopumped. Another sign that the vacuum in the trap was degraded is the absence of data points between 2.4 and 2.8 h. The pressure was then so high that the plasma either did not survive until the end of the cycle or was not trapped to begin with.

The plasma parameters were not constant as the trap warmed and off-gassed because emission from the electron source changes at higher pressure; in particular, the BaO cathode is poisoned by hydrogen. When the gas load was relatively high, N and r_p were found to

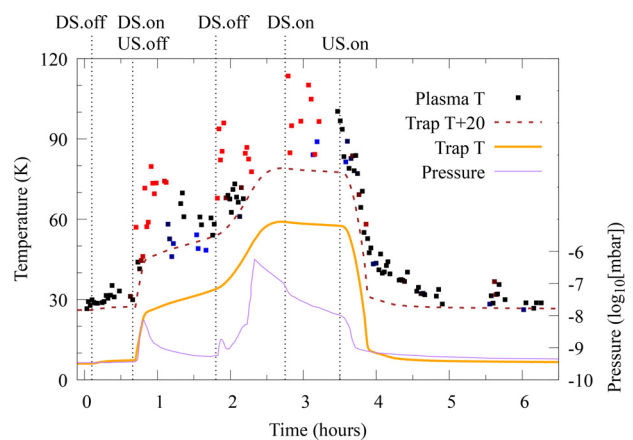


FIG. 4. Plasma temperature measurements taken while trap III was warmed up and cooled back down. Trap temperature and pressure (outside the trap) were monitored simultaneously. The upstream (US) and downstream (DS) coldheads were both running for several days at the start of the scan. The time that each coldhead was turned off or on is indicated by dashed lines, labeled at the top of the graph. Point coloring indicates plasma space charge, with black as nominal, red being relatively more, and blue less (see the text). The nominal plasma parameters were $N = 31 \times 10^6$, $n = 3.2 \times 10^8 \text{ cm}^{-3}$, $r_p = 1.0 \text{ mm}$, and $L_p = 4.0 \text{ cm}$.

increase significantly (factor of 2–6); this was also correlated with higher temperature. In response, the electron load was continually tuned to bring the number of electrons and plasma radius back toward their original value. To give some indication of these deviations, the points on Fig. 4 are color coded by the space charge. This is the value of the vacuum well depth at the moment that the first particles begin to escape (when the plasma is slowly released), and it correlates positively with the number of electrons in the plasma. Black points correspond to plasma with a space charge between 6 and 8 V. Blue points mean the plasma was smaller, that is, space charge <6 V; red points mean the plasma was larger.

The cycle-to-cycle variation under variable gas load caused significant spread in the temperature data. Still, one can make the conservative assumption that for each cluster of data in a small range of temperature and pressure, and the lowest points are representative of the lowest temperatures achievable in the trap at that temperature and pressure. This “minimum temperature” seems to follow a curve at an offset of about 20 K above the trap temperature T_b , in spite of significant variation in the pressure around, and most likely within, the trap.³¹ Even under the worst possible vacuum conditions (close to the point where the plasma temperature could not be diagnosed at all), the minimum plasma temperature in trap III (80 K) was much closer to the electrode temperature (60 K at that time) than in traps I and II.

D. Magnetic field

The plasma may be heated by applying broadband radio frequency noise to an electrode.³² Providing that the noise is applied for a time, which is long compared to the collisional relaxation time, the plasma temperature can be raised reproducibly to any value up to a few eV. When the noise is switched off, the plasma cools back down toward T_f according to Eq. (1). One can measure Γ by fitting the slope (on a semi-log plot) of the cooling curve, T vs t , where t is the time between turning off the noise and measuring the plasma temperature.³³ Such measurements have been performed extensively in traps II and III. Typical results for trap III are shown in Fig. 5.

The cooling rate Γ depends on the magnetic field B , and the latter can be reduced by ramping down the current in the cusp magnet. By repeating the cooling curve measurement for different values of B , 11 pairs of fit parameters $\{\Gamma, T_f\}$ were obtained. These are shown in the inset to Fig. 5. Using Eq. (2), the data are fit by a line with slope $H = 11 \pm 1$ K/s and y -intercept $T_b = 12 \pm 2$ K. However, the accuracy of this result depends on the approximation that H is constant when B is varied. In fact, lower B implies faster plasma expansion. The additional expansion heating would make H a function of $1/\Gamma$ so that the data would curve upward instead of following a line. In this situation, a linear fit tends to overestimate H (for small $1/\Gamma$) and underestimate T_f .

The tendency for faster plasma expansion at low B was intensified by the fact that the cusp field’s symmetry axis also depends on B . This is likely a combination of two effects: (1) nonlinearity due to magnetic saturation in the hot-rolled steel shield enclosing the cusp magnet and (2) a different distribution of supercurrents in the anti-Helmholtz coils chosen to reach lower B at the plasma. The angle between the symmetry axes of \mathbf{E} and \mathbf{B} was tuned to be less than 1 mrad for $B = 1.9$ T. The alignment was not retuned when B was changed, resulting in a misalignment of approximately 3 mrad for the lowest B value studied. The plasma expansion time was 8500 s for the highest value of B and 900 s for the lowest, corresponding to expansion

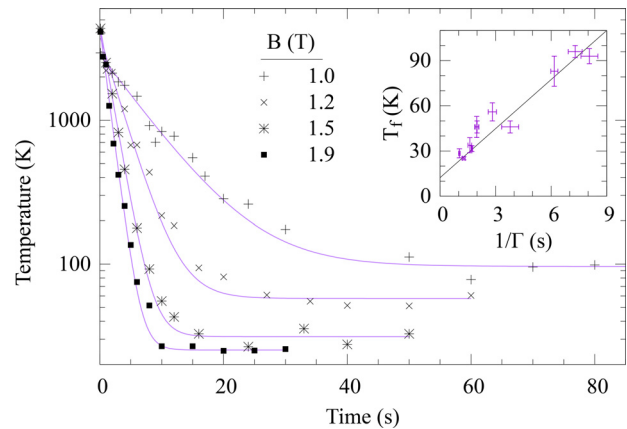


FIG. 5. Cooling curves for different values of the magnetic field. The plasma temperature falls initially as $T \sim \exp[-\Gamma t]$ and asymptotes to a final temperature T_f . The fit curves are used to determine Γ and T_f . Eleven such fit-parameter pairs are plotted in the inset. The trendline has slope H and y -intercept T_b , following Eq. (2). The same plasma preparation was used for these scans as for Fig. 4; at $B = 1.9$ T, the plasma parameters were also the same. (1.9 T is a mean value; B varied by about 10% over the length of the plasma.) At lower magnetic field, the electron load was adjusted to keep N close to its nominal value. The mean and standard deviation for the complete data set are $N = 31 \pm 5 \times 10^6$ electrons and $r_p = 1.0 \pm 0.2$ mm, where greater values of r_p correlated with lower B .

heating rates 1 and 12 K/s, respectively. To further complicate matter, the slowest cooling was observed at an intermediate field value where cooling was suppressed well below the free-space value, presumably by cavity-resonant effects. This explains why the constant best-fit value $H = 11$ K/s does not fit the data perfectly.

In view of these limitations, the trendline in Fig. 5 does not provide a reliable estimate of either the heating rate H or the base temperature T_b . However, the fit parameters are useful for providing bounds on these quantities. In particular, supposing that H does not decrease when B is decreased, then H cannot be much more than the fitted value of 11 K/s; this agrees with the heating rate estimated in the preceding paragraph from the expansion rate at low B . This upper bound on H , combined with the high-field points at $1/\Gamma \approx 1$ s and $T_f \approx 25$ K, allows a lower bound to be placed on T_b at the fitted value $T_b = 12 \pm 2$ K. Meanwhile, an upper bound for T_b is the minimum observed $T_f \approx 25$ K. These measurements therefore establish that $12 \lesssim T_b < 25$ K in trap III.

IV. DISCUSSION

The time dependence of the plasma temperature in trap III is well modeled by Newton’s law of cooling, Eq. (1), with an effective background temperature $T_b \approx 20$ K. Of the three trap designs studied, only trap III, which was engineered to contain the cyclotron radiation of the plasma, could produce plasma with T_f anywhere near the trap temperature T_b . Cooling curves taken in traps I and II asymptote to much higher T_f , implying higher effective background temperature T_b (for equivalent H). For example, in Ref. 22 a measurement similar to Fig. 5 was performed in trap II a and yielded $T_b \sim 100$ K (130 K if the adiabatic corrections discussed in Appendix A are applied).

The best explanation for these observations is that the copper meshes in trap III reflected room-temperature radiation at the

cyclotron frequency, confining cyclotron radiation to the coldest part of the trap and fixing T_b at the temperature of the cryogenic absorbing material. However, the meshes were not the only feature distinguishing trap III from the others. Other differences among the traps are considered in [Appendix C](#).

Coupling to room-temperature radiation is a general problem for the cooling of charged particles in cryogenic open-ended traps. Temperatures as low as those reported here are seldom observed without applying active techniques such as laser or evaporative cooling. The few exceptions involve traps where room temperature microwave radiation was reduced, excluded from the cryogenic region, or otherwise rendered insignificant:

1. The BASE collaboration achieved sub-Kelvin cyclotron energy for a single antiproton in a Penning trap with a 2 T magnetic field.³⁴ The trap was entirely enclosed by surfaces cooled to 6 K and sealed with indium. Similarly, a small Penning trap (1 cm³ surrounded by electrodes), nominally at 1.6 K in a 5 T field, was used to cool a single electron to 5 K via cyclotron radiation. The cyclotron motion of the electron was further cooled to 0.85 K by suppressing the cyclotron coupling to the electrodes (detuning from a cavity resonance) and using feedback from a cryogenic amplifier.³⁵
2. The thesis of Beck¹⁶ reported plasma containing $N \sim 10^7$ electrons cooled as low as $T \approx 30$ K. As in the preceding example, the trap was pinched off and indium sealed. The trap was immersed in helium and operated at 6 T.
3. The ALPHA collaboration reported the cooling of plasma containing 2.6×10^6 positrons to $T \approx 50$ K via cyclotron radiation in a 3 T magnetic field¹² (more recent measurements³⁶ suggested a lower temperature $T \sim 20$ K; however, this temperature was measured after an adiabatic cooling step and therefore does not describe the steady state of the plasma). The helium-cooled trap had open endcaps in order to permit axial transport of electrons, positrons, antiprotons, and ions. The apertures enclosing the trapping region had a measured temperature of 6–7 K and had inner diameter $d \approx 10$ mm. In addition to these apertures, access for an off-axis laser beam was provided through a 11-mm-long diameter port containing a resistively coated ceramic microwave absorber.³⁷
4. The thesis of Hunter³⁸ reported electron plasma cooled to within a few degrees of trap temperature (9 K) for the entire range $10^4 < N < 10^7$. The trap was open at both ends with 10-mm copper apertures. The plasma was cooled using cyclotron-cavity resonance in a 1 T field. On resonance, the coupling to the cavity mode was typically 20 times higher than the Larmor rate, which limited the influence of modes external to the trap by a similar factor.

The antihydrogen groups at CERN (AEgIS, ALPHA, ASACUSA, and GBAR) cannot perform their experiments in a hermetically sealed cryogenic trap. The results obtained so far by the ALPHA collaboration appear to be a compromise between low temperature and finite acceptance. Groups like AEgIS and ASACUSA cannot make the same compromise as ALPHA, for they require a large opening from the cryogenic region in order for antihydrogen atoms to escape. These groups have struggled for many years to achieve sufficiently cold plasma and may ultimately conclude that it is impossible to do so

without blocking room temperature microwave radiation with methods similar to those presented here. The ALPHA and GBAR groups might also benefit from the improved access and shielding provided by a larger aperture covered in a mesh, which blocks microwaves. In contrast to a simple copper mesh, the absorber used for ALPHA's laser port has a limited range of application due to its large aspect ratio and small diameter. Furthermore, the device did not attenuate at sufficiently high frequency for cooling in magnetic fields greater than 1 T.

V. CONCLUSION

The final temperature of the electron plasma held in ASACUSA's Cusp trap was anomalously high (trap I) and even increased after a significant reduction in trap temperature (trap II). The addition of fine copper meshes (trap III) provided an effective barrier against microwaves entering the trap at the cyclotron frequency and coincided with a dramatic reduction in plasma temperature.

The effect was found to be independent of many variations in plasma parameters. A movable thermal shield permitted a partial study of the apparent heating in a system without meshes. The plasma was consistently 20 K hotter with the shield open, for $2 < N < 12 \times 10^6$ electrons. Earlier work had found that the difference was nearly 20 K for four different plasma positions (with different cooling and expansion rates). Reducing the upstream aperture of this trap by a factor of two reduced the minimum achievable plasma temperature by about 40 K. For the system with meshes, a further reduction of about 80 K was witnessed over a wide range of plasma density (factor of 10), radius (factor of 2), and number of electrons (factor of 40).

The results of the present study offer strong support for the hypothesis that the meshes allow the plasma to cool to lower temperature by blocking radiation that could couple the plasma to warmer regions of the apparatus. This finding enables the formation of magnetized cryogenic electron plasma in a trap with large solid angle acceptance to room-temperature apparatus. There is no reason to expect that a positron plasma would cool differently than the electron plasma used in this study. Cold positrons are a prerequisite for ASACUSA's planned measurement of the hyperfine splitting in ground-state antihydrogen,³⁹ which requires a large acceptance for a diffuse antihydrogen beam to exit the trap. Theoretically,⁴⁰ a positron plasma with properties similar to the electron plasma described here could be used to generate two orders of magnitude more ground-state antihydrogen than has previously been achieved in ASACUSA's Cusp trap.

ACKNOWLEDGMENTS

The meshes and microwave absorbers used in trap III were proposed by Fritz Caspers of CERN's RF group. Engineering design and procurement for trap III were undertaken chiefly by Doris Pristauz-Telsnigg of the Stefan Meyer Institute. This work was supported by the Austrian Science Fund (FWF) Grant Nos. P 32468, W1252-N27, and P 34438; the JSPS KAKENHI Fostering Joint International Research Grant No. B 19KK0075; the Grant-in-Aid for Scientific Research Grant No. B 20H01930; Special Research Projects for Basic Science of RIKEN; Università di Brescia and Istituto Nazionale di Fisica Nucleare; and the European Union's Horizon 2020 research and innovation program under the Marie Skłodowska-Curie Grant Agreement No. 721559.

AUTHOR DECLARATIONS

Conflict of Interest

The authors have no conflicts to disclose.

Author Contributions

H.H., E.D.H., A.L., V.Mä., D.J.M., N.K., and M.T. developed and operated the traps used for plasma cooling. E.D.H., V.Kl., A.L., V.Mä., D.J.M., M.S., and J.Z. developed the new cold bore for Trap III. Trap upgrades were carried out by C.A., H.B., G.C., R.F., M.G., G.G., A.G., E.D.H., A.L., M.L., V.Mä., G.M., S.M., D.J.M., L.N., M.R., V.T., A.W., E.W., T.W., and J.Z. All authors critically reviewed and approved the final version of the manuscript. The authors of this article are members of the ASACUSA-Cusp collaboration. **Claude Amsler:** Writing – review and editing (supporting). **Eric D Hunter:** Writing – original draft (lead). **Carina Killian:** Writing – review and editing (supporting). **Victoria Kletzl:** Writing – review and editing (supporting). **Viktoria Kraxberger:** Writing – review and editing (supporting). **Naofumi Kuroda:** Writing – review and editing (supporting). **Andreas Lanz:** Writing – review and editing (supporting). **Marco Leali:** Writing – review and editing (supporting). **Volhard Maeckel:** Writing – review and editing (supporting). **Giancarlo Maero:** Writing – review and editing (supporting). **Chloe Malbrunot:** Writing – review and editing (supporting). **Horst Breuker:** Writing – review and editing (supporting). **Valerio Mascagna:** Writing – review and editing (supporting). **Yasuyuki Matsuda:** Writing – review and editing (supporting). **Stefano Migliorati:** Writing – review and editing (supporting). **Daniel James Murtagh:** Writing – review and editing (supporting). **Yugo Nagata:** Writing – review and editing (supporting). **Amit Nanda:** Writing – review and editing (supporting). **Lilian Nowak:** Writing – review and editing (supporting). **Eleonora Pasino:** Writing – review and editing (supporting). **Massimiliano Romé:** Writing – review and editing (supporting). **Martin C Simon:** Writing – review and editing (supporting). **Svetlana Chesnevskaya:** Writing – review and editing (supporting). **Minori Tajima:** Writing – review and editing (supporting). **Valerio Toso:** Writing – review and editing (supporting). **Stefan Ulmer:** Writing – review and editing (supporting). **Luca Venturelli:** Writing – review and editing (supporting). **Alina Weiser:** Writing – review and editing (supporting). **Eberhard Widmann:** Writing – review and editing (supporting). **Tim Hilmar Wolz:** Writing – review and editing (supporting). **Yasunori Yamazaki:** Writing – review and editing (supporting). **Johann Zmeskal:** Writing – review and editing (supporting). **Giovanni Costantini:** Writing – review and editing (supporting). **Rafael Ferragut:** Writing – review and editing (supporting). **Marco Giammarchi:** Writing – review and editing (supporting). **Angela Gligorova:** Writing – review and editing (supporting). **Giulia Gosta:** Writing – review and editing (supporting). **Hiroyuki Higaki:** Writing – review and editing (supporting).

DATA AVAILABILITY

The data that support the findings of this study are available from the corresponding author upon reasonable request.

APPENDIX A: SYSTEMATIC UNCERTAINTIES

The plasma must be dumped out of the trap in order to measure its temperature with the parallel energy analysis technique.²⁸

The act of dumping the plasma entails non-trivial changes to the plasma length, space charge, and temperature.¹⁶ In particular, as the confinement is reduced, the plasma becomes longer, causing an adiabatic decrease in temperature as well as a reduction in space charge. The uncertainties involved in modeling the evolution of the plasma, as the confinement is reduced and particles begin to escape, translate into significant systematic uncertainty in the measured temperature.

Adiabatic expansion causes the temperature to fall as $T_2/T_1 = (L_2/L_1)^{2/f}$, where the effective number of degrees of freedom f should lie in a range between 1 and 4, depending on whether the length changes quickly compared with the collision time (for axial-transverse equilibrium) and whether the potential (including space charge) is harmonic or flat with steep walls. For the data presented in this article, the dump time was longer than the collisional relaxation time ($f=3$ or $f=4$) and the Debye length $\lambda_D < 0.1$ mm, implying the electrostatic potential was always well shielded and therefore flat ($f=3$). The ratio $L_2/L_1 \sim 2$ for much of the data presented in Sec. III, meaning that those plasmas were typically a factor $2^{2/3} \approx 1.6$ hotter before the well was opened for the diagnostic.

This effect is seldom included in the analysis of plasma temperature. For example, Ref. 36 claims to have achieved temperatures as low as 7 K using a new technique for sympathetically cooling positrons. In fact, the positron plasma was cooled in a deep well (70 V on-axis) spanning only one electrode; although the paper does not provide sufficient information to determine the ratio L_2/L_1 exactly, simple estimates based on the electrode geometry suggest a value of 3 or more, implying that the positron temperature was at least a factor of 2 higher (i.e., 14 K) prior to adiabatic expansion.

There are also effects, which cause the diagnostic to read higher than the true plasma temperature. It was recognized early on¹⁶ that the escaping charge would cause the space charge of the remaining plasma to fall. This lowers the effective dump rate because reduced space charge means more energy is required for a particle to reach the top of the well and escape. A related effect has come to the community's attention more recently,⁴¹ namely, that the increasing plasma length during the dump also causes the space charge to fall. This effect would cause the plasma in the present work to appear 20% – 25% hotter than it really was, assuming that the orbits of all particles increased proportionally.

The calculation of these effects requires accurate characterization of several parameters (number, radius, length, density, and space charge) for every plasma tested. Like the temperature, the plasma number and radius both suffer from systematic errors, which exceed the statistical uncertainty; meanwhile, the length and density are derived from these using a numerical (Poisson) solver.⁴² Even if all of the parameters were known precisely, significant uncertainty would remain due to model assumptions. In addition to those described above, it is worth noting that the profile of a non-neutral plasma in a magnetic mirror field is distorted away from the ellipsoid to something resembling a cone.⁴³ This and other possible consequences of the mirror field were not included in the analysis which follows.

Figure 6 presents a reanalysis of the temperature data, which was shown in Fig. 2. Whereas Fig. 2 reported the temperatures with no corrections, Fig. 6 includes the $(L_2/L_1)^{2/3}$ correction for adiabatic cooling during the diagnostic. While this is not the only

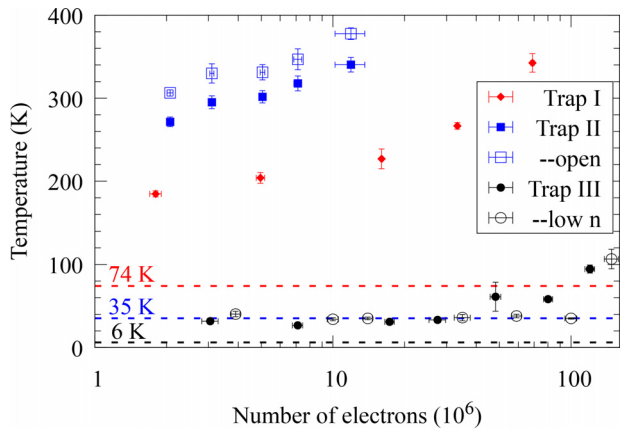


FIG. 6. Reanalysis of the data shown previously in Fig. 2, increasing the temperatures by a factor $(L_2/L_1)^{2/3}$. The initial length L_1 is derived numerically from the measured radius and number of electrons, while the final length L_2 is inferred based on the shape of the confinement potential at the moment when particles begin to escape the well during the temperature diagnostic.

correction that should be applied, the other corrections tend to counteract this one, so that comparison of the two figures serves to illustrate the size of the effects discussed in this section: typically a factor of 1.5. None of this changes the conclusion of the article.

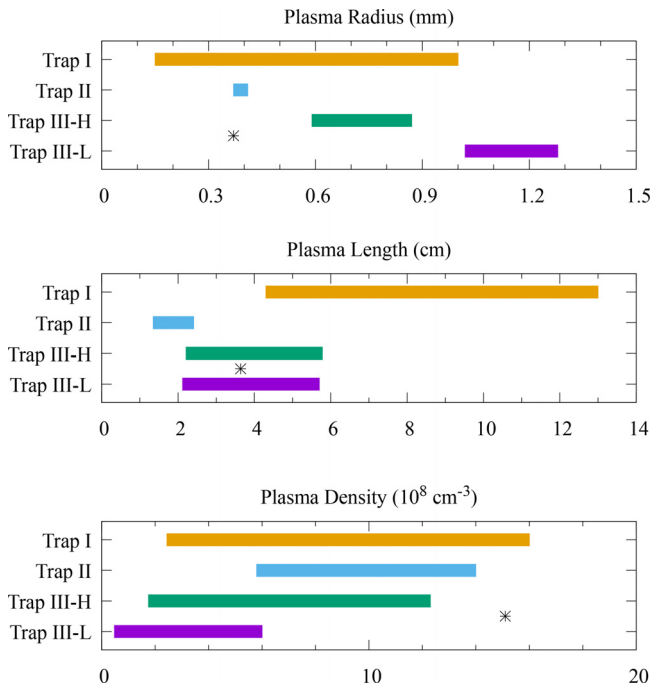


FIG. 7. Plasma parameter ranges for the data presented in Fig. 2. The black stars give the values chosen for the trap III plasma of Fig. 3. The suffix -H or -L stands for the high- or low-density data set in trap III. Plasma radius was measured via a photo taken after fast dump onto the MCP-phosphor assembly. Plasma length and density were determined by a self-consistent Poisson-Boltzmann code,⁴² which takes the radius, number of electrons, and confinement potentials as input.

Indeed, adiabatic corrections enhance the disparity in observed plasma temperature between the traps.

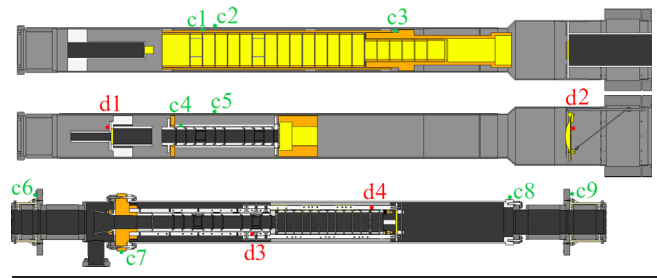
Figure 7 shows the ranges (measured or calculated) of parameters for the plasma studied in Fig. 2. The largest corrections due to adiabatic expansion occurred for the trap II data set. Figure 7 shows that this plasma was also the shortest. Trap II plasma was held in a deep, single-electrode well. Such plasma is typically more susceptible to these systematic errors than a longer plasma, which spans several electrodes.

APPENDIX B: TEMPERATURE OF THE APPARATUS

The trap temperature T_t was measured by sensors mounted either directly on an electrode (trap II) or on the high-conductivity electrode support structure (traps I and III) (see Table II). A simple heat balance calculation suggests that the sensors used to define T_t were generally within 1 K of the electrode temperature for all traps studied. For trap I, the support structure was made of high-purity copper (OFHC) and connected via short wires (~2 cm, KAP-060) clamped to a thin plate (2 mm, AlN) on each electrode. The heat load for trap I electrodes was estimated⁴⁴ at 5–10 mW and would correspond to a temperature differential of 1 K over the wire. For trap III, the thermal connection for a typical electrode is illustrated in Fig. 8. The radiative heat load for trap III electrodes was everywhere less than 10 mW, being lower for electrodes farther downstream. A 10 mW load would produce a 0.25 K differential on the configuration shown in Fig. 8. If AlN had been used instead of Kapton, the differential could have been even lower.

TABLE II. List of temperature sensors and their values for the three traps. (Here, the version of trap II with reduced upstream solid angle, trap II a, is shown.) Sensors are labeled “c” for Lakeshore Cernox or “d” for diode type sensors. Due to some miscommunication, the Cernox sensors installed in trap III had not been calibrated; for those sensors, the upper and lower temperature bounds are given for the resistance measured. The sensors used to define T_t have been underlined in the table.

Trap I	<u>c1</u>	c2	c3			
Temp. (K)	74 ± 6	65 ± 3	77 ± 6			
Trap II	d1	<u>c4</u>	c5	d2		
Temp. (K)	63 ± 1	33 ± 2	58 ± 2	198 ± 3		
Trap III	c6	c7	<u>d3</u>	d4	c8	c9
Temp. (K)	23–85	1–8	6.2 ± 0.5	5.4 ± 0.5	8–13	30–100



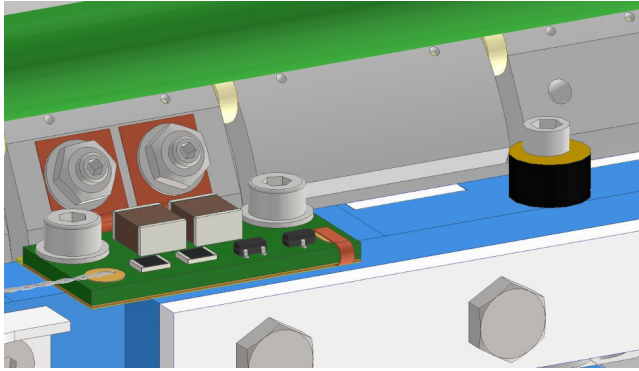


FIG. 8. Cooling mechanism and electrical connection for the electrodes in trap III. CAD software was used to render temperature sensor (black), aluminum cooling bar (blue), cryogenic filterboard (green), and connection to electrode (gray) via copper cooling pad (brown). The copper pad is clamped between the filterboard and the aluminum bar. It is isolated electrically from the bar by a thin piece of Kaptan tape.

This work seeks to demonstrate the importance of coupling to objects other than the trap electrodes. While the electrodes typically occupy over 99% of the solid angle seen by the plasma, they are often made of material, which is not sufficiently resistive to damp the radiation generated by the plasma. For example, the stainless steel vacuum chamber of traps I and II was at least 100 times more resistive than the aluminum electrodes of traps II and III (and possibly 1000 times more resistive than the cryogenic high-conductivity copper electrodes of trap I). In this sense, the electrodes merely reflect the cyclotron radiation, redirecting it toward more resistive, potentially warmer surfaces. For trap III, the sensor readings (Table II) suggest that the entire region enclosed by the meshes was below 13 K. Less precise information is available for traps I and II. For those traps, the stainless steel vacuum chamber probably sustained a thermal gradient of order 100 K per meter from the cooling contact point (close to c4 on the upstream side) to the downstream side. This estimate is based on two measurements: (1) the difference between sensors c4 and c5 and (2) the temperature of the downstream thermal shield, measured by sensor d1. Neither of these measurements gives much certainty, since (1) the temperature gradient for steel cooled to less than 35 K at one point and heated at both ends must be nonlinear as a function of position and (2) the thermal shield was subjected to ~ 100 mW of thermal radiation from farther downstream.

APPENDIX C: OTHER DIFFERENCES BETWEEN THE TRAPS

Noise on the electrodes can heat the plasma. Noise was minimized for all configurations by using low-speed amplifiers, low-pass filters enclosed in a thick aluminum box mounted directly to the vacuum feedthrough, and cryogenic low-pass filters close to the electrodes. For trap I, the cryogenic filters were bypassed by diodes in order to allow fast high-amplitude signals to pass. However, because this design also admits noise any time the electrode bias changes in a time comparable to the filter time constant, the diode bypass was removed in traps II and III for all but the outermost electrode (which is used for catching and therefore must be pulsed). For trap I, signals were carried through vacuum a distance of

approximately 1.0 m on homemade stainless steel coaxial cables, with the outer shield grounded at the trap side. For trap II, the same distance was spanned by Lakeshore Quad-Twist™ phosphor bronze twisted pair wire, with every other wire grounded at both sides. For trap III, more Quad-Twist wire was used, with the distance traversed in vacuum reduced by a factor of two.

The precautions taken against high-frequency noise are ineffectual against noise at a lower frequency ($f < 100$ kHz). Such noise can heat the plasma by changing the plasma length on timescales comparable to the axial-transverse equilibration time, such that entropy is produced in the collisional exchange of energy between the axial and transverse degrees of freedom.¹⁴ Evidently, this noise source did not significantly heat the trap III plasma. Since trap II used essentially the same amplifier, filter, and feedthrough designs as trap III, there is no reason to suspect that low-frequency noise would have been significant for trap II and not for trap III.

The inner diameter of the electrodes in trap I was 80 mm, while the inner diameter of the electrodes in traps II and III was 34 mm. The electrodes of trap I were gold-coated, while the electrodes of traps II and III were coated first in gold, then in colloidal graphite (Electron Microscopy Systems No. 12660). The inner surfaces of the cold bore housing trap III were also darkened with the alcohol-graphite solution, whereas some of the surfaces for traps I and II were highly reflective.

Trap III was installed as part of a new cold bore with two new coldheads. By contrast, the electrode stacks of traps I and II were placed in an older cold bore with only one functioning coldhead. For trap I, the inactive coldhead constituted a heat load on the cold bore. For trap II, the broken coldhead was removed from the system; that is why trap II was colder than trap I. Thus, for traps I and II, the temperature of the vacuum chamber increased in the downstream direction, approaching 200 K in the vicinity of the downstream aperture. This may account for the smallness of the effect of closing the movable shield in trap II. It would also imply that cryopumping was much less effective in traps I and II. However, the inefficient cryopumping may have been compensated by the fact that traps I and II were pumped from upstream and downstream by non-evaporable getter pumps, with the typical pressure at the downstream side being less than 3×10^{-10} mbar, whereas trap III was only pumped on the upstream side.

APPENDIX D: LOADING AND DUMPING THROUGH THE MESH

The presence of a mesh at the upstream side of the trap has consequences for particle loading as well as the dump diagnostics (charge counting, imaging, and temperature). The nominal 79% transparency implies that 21% of the particles coming into or out of the trap are absorbed by the mesh. The mesh was sprayed with colloidal graphite and firmly clamped to ground around the circumference to mitigate ensuing charge-up effects.

The charge measurements, which determine N for trap III, were all scaled assuming a transmission factor 0.79. The true fraction of passing particles could be greater or less than the geometrical transparency of the mesh. For instance, the particles oscillate due to cyclotron motion while traversing the mesh. The antiproton beam described in Ref. 45 had 0.2 eV transverse energy and 1.5 eV axial energy. The corresponding cyclotron radius and cyclotron

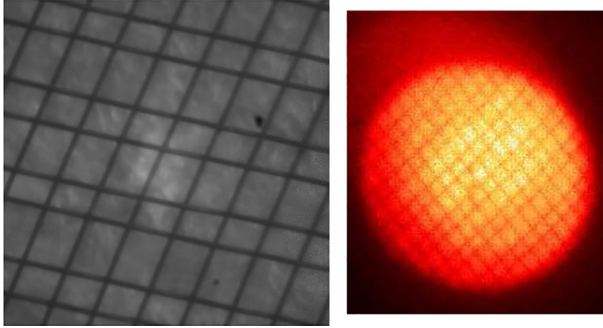


FIG. 9. The fine copper mesh. Left side: picture of a sample under a microscope, after graphite coating. Right side: image of the plasma, showing the mesh pattern where electrons coming out of the trap were absorbed.

frequency are 0.3 mm and 2 MHz in the cusp field at the location of the upstream mesh. At 1.5 eV, the antiproton would take about 3 ns to traverse the 0.03 mm mesh in the axial direction. During that time, the cyclotron motion would carry it 0.01 mm in the transverse direction. The mesh would be effectively 30% thicker for such a low energy beam of antiprotons.

The imaging diagnostic is partly benefited by the presence of the mesh. Figure 9 demonstrates that the mesh pattern can be imaged by the plasma as it passes out of the trap on its way to the imaging detector. This provides a cross-check of the linear scaling factor used to determine the plasma radius. The scaling factor is normally assumed to be equal to the square root of the mirror ratio between the trap and the detector. That assumption is only valid for magnetized particles in the absence of drifts. It is probably a good assumption in the strong field between the trap and the mesh, but a questionable assumption in the low magnetic field and potentially large electric fields in the vicinity of the MCP detector. Using the mesh pattern as a reference, the scaling factor used previously was found to be too great by a factor 25/18. Thus, in the absence of the mesh, one would have assumed the plasma to be $(25/18)^2 \sim 1.5$ times denser than it really was.

For the temperature diagnostic, it is desirable that the mesh wires to be smaller than the Debye length of the plasma. This is because the first particles to escape come from a cylinder having a radius of approximately $2\lambda_D$.⁴⁶ In the extreme case where a single wire covered this “Debye cylinder,” the earliest-escaping particles would not reach the detector. The signal would come from later-arriving particles, which are hampered by the declining space charge of the plasma; in the absence of other effects, this would increase the measured plasma temperature. For the trap III plasma having the smallest Debye length $\lambda_D \approx 20 \mu\text{m}$, the cylinder from which particles initially escape would have been two or three times as big as a mesh wire. The case is actually less serious than that because, as mentioned in the preceding paragraph, the plasma is stretched out transversely due to the mirror ratio between the trap and the mesh. Effectively, the cylinder in question would have been five or six times as thick as a mesh wire even in the worst case.

REFERENCES

- ¹M. Amoretti, C. Amsler, G. Bonomi, A. Bouchta, P. Bowe, C. Carraro, C. L. Cesar, M. Charlton, M. J. T. Collier, M. Doser *et al.*, “Production and detection of cold antihydrogen atoms,” *Nature* **419**, 456–459 (2002).
- ²G. Gabrielse, N. S. Bowden, P. Oxley, A. Speck, C. H. Storry, J. Tan, M. Wessels, D. Grzonka, W. Oelert, G. Schepers *et al.*, “Background-free observation of cold antihydrogen with field-ionization analysis of its states,” *Phys. Rev. Lett.* **89**, 213401 (2002).
- ³Y. Enomoto, N. Kuroda, K. Michishio, C. Kim, H. Higaki, Y. Nagata, Y. Kanai, H. Torii, M. Corradini, M. Leali *et al.*, “Synthesis of cold antihydrogen in a cusp trap,” *Phys. Rev. Lett.* **105**, 243401 (2010).
- ⁴S. Maury, “The antiproton decelerator: AD,” *Hyperfine Interact.* **109**, 43–52 (1997).
- ⁵M. Ahmadi, B. X. R. Alves, C. J. Baker, W. Bertsche, E. Butler, A. Capra, C. Carruth, C. L. Cesar, M. Charlton, S. Cohen *et al.*, “Observation of the hyperfine spectrum of antihydrogen,” *Nature* **548**, 66–69 (2017).
- ⁶M. Ahmadi, B. X. R. Alves, C. Baker, W. Bertsche, A. Capra, C. Carruth, C. L. Cesar, M. Charlton, S. Cohen, R. Collister *et al.*, “Characterization of the 1s–2s transition in antihydrogen,” *Nature* **557**, 71–75 (2018).
- ⁷R. Bluhm, V. A. Kostelecký, and N. Russell, “CPT and Lorentz tests in hydrogen and antihydrogen,” *Phys. Rev. Lett.* **82**, 2254 (1999).
- ⁸A. Kellerbauer, M. Amoretti, A. Belov, G. Bonomi, I. Boscolo, R. Brusa, M. Büchner, V. Byakov, L. Cabaret, C. Canali *et al.*, “Proposed antimatter gravity measurement with an antihydrogen beam,” *Nucl. Instrum. Methods Phys. Res., Sect. B* **266**, 351–356 (2008).
- ⁹P. Perez, D. Banerjee, F. Biraben, D. Brook-Roberge, M. Charlton, P. Cladé, P. Comini, P. Crivelli, O. Dalkarov, P. Debu *et al.*, “The gbar antimatter gravity experiment,” *Hyperfine Interact.* **233**, 21–27 (2015).
- ¹⁰W. A. Bertsche, “Prospects for comparison of matter and antimatter gravitation with alpha-g,” *Philos. Trans. R. Soc. A* **376**, 20170265 (2018).
- ¹¹M. Dine and A. Kusenko, “Origin of the matter-antimatter asymmetry,” *Rev. Mod. Phys.* **76**, 1 (2003).
- ¹²M. Ahmadi, B. X. R. Alves, C. J. Baker, W. Bertsche, E. Butler, A. Capra, C. Carruth, C. L. Cesar, M. Charlton, S. Cohen *et al.*, “Antihydrogen accumulation for fundamental symmetry tests,” *Nat. Commun.* **8**, 681 (2017).
- ¹³F. Robicheaux, “Atomic processes in antihydrogen experiments: A theoretical and computational perspective,” *J. Phys. B: At., Mol. Opt. Phys.* **41**, 192001 (2008).
- ¹⁴B. Beck, J. Fajans, and J. Malmberg, “Measurement of collisional anisotropic temperature relaxation in a strongly magnetized pure electron plasma,” *Phys. Rev. Lett.* **68**, 317 (1992).
- ¹⁵J. R. Danielson, D. H. E. Dubin, R. G. Greaves, and C. M. Surko, “Plasma and trap-based techniques for science with positrons,” *Rev. Mod. Phys.* **87**, 247 (2015).
- ¹⁶B. R. Beck, “Measurement of the magnetic and temperature dependence of the electron-electron anisotropic temperature relaxation rate,” Ph.D. thesis (University of California, San Diego, 1990).
- ¹⁷G. B. Andresen, M. D. Ashkezari, M. Baquero-Ruiz, W. Bertsche, P. D. Bowe, E. Butler, C. L. Cesar, S. Chapman, M. Charlton, J. Fajans *et al.*, “Evaporative cooling of antiprotons to cryogenic temperatures,” *Phys. Rev. Lett.* **105**, 013003 (2010).
- ¹⁸J. Malmberg, C. Driscoll, B. Beck, D. Eggleston, J. Fajans, K. Fine, X.-P. Huang, and A. Hyatt, “Experiments with pure electron plasmas,” *AIP Conf. Proc.* **175**, 28–74 (1988).
- ¹⁹M. R. Natisin, J. R. Danielson, and C. M. Surko, “Formation of buffer-gas-trap based positron beams,” *Phys. Plasmas* **22**, 033501 (2015).
- ²⁰N. Evetts, I. Martens, D. Bizzotto, D. Longuevergne, and W. N. Hardy, “Open microwave cavity for use in a Purcell enhancement cooling scheme,” *Rev. Sci. Instrum.* **87**, 104702 (2016).
- ²¹E. Kur, F. Robicheaux, N. Evetts, J. Fajans, A. Guerra, IV, W. N. Hardy, E. D. Hunter, Z. T. Schroeder, and J. S. Wurtele, “Computational and theoretical analysis of electron plasma cooling by resonant interaction with a microwave cavity,” *Phys. Plasmas* **27**, 082101 (2020).
- ²²E. Hunter, C. Amsler, H. Breuker, S. Chesnevskaya, G. Costantini, R. Ferragut, M. Giammarchi, A. Gligorova, G. Gosta, H. Higaki *et al.*, “Minimizing plasma temperature for antimatter mixing experiments,” in *EPJ Web of Conferences* (EDP Sciences, 2022), Vol. 262, p. 01007.
- ²³M. R. Natisin, J. R. Danielson, and C. M. Surko, “Positron cooling by vibrational and rotational excitation of molecular gases,” *J. Phys. B: Atomic, Molecular and Optical Physics* **47**(22), 225209 (2014).

- ²⁴H. Saitoh, A. Mohri, Y. Enomoto, Y. Kanai, and Y. Yamazaki, "Radial compression of a non-neutral plasma in a cusp trap for antihydrogen synthesis," *Phys. Rev. A* **77**, 051403 (2008).
- ²⁵D. Anke, H.-D. Brüns, B. Deserno, H. Garbe, K.-H. Gonschorek, P. Hansen, J. L. ter Haseborg, S. Keim, S. Kohling, K. Rippl *et al.*, *Elektromagnetische Verträglichkeit: Grundlagen, Analysen, Maßnahmen* (Springer-Verlag, 2013).
- ²⁶F. Caspers, "Experience with UHV-compatible microwave absorbing materials at CERN," Technical Report No. CM-P00059508, 1993.
- ²⁷E. D. Hunter, J. Fajans, N. A. Lewis, A. P. Povilus, C. Sierra, C. So, and D. Zimmer, "Plasma temperature measurement with a silicon photomultiplier (sipm)," *Rev. Sci. Instrum.* **91**, 103502 (2020).
- ²⁸D. L. Eggleston, C. F. Driscoll, B. R. Beck, A. W. Hyatt, and J. H. Malmberg, "Parallel energy analyzer for pure electron plasma devices," *Phys. Fluids B* **4**, 3432–3439 (1992).
- ²⁹M. Ahmadi, B. X. R. Alves, C. J. Baker, W. Bertsche, A. Capra, C. Carruth, C. L. Cesar, M. Charlton, S. Cohen, R. Collister *et al.*, "Enhanced control and reproducibility of non-neutral plasmas," *Phys. Rev. Lett.* **120**, 025001 (2018).
- ³⁰J. Malmberg and C. Driscoll, "Long-time containment of a pure electron plasma," *Phys. Rev. Lett.* **44**, 654 (1980).
- ³¹Without knowing the pressure inside the trap, it is difficult to exclude the possibility of unintentional "buffer-gas" cooling on the residual gas evolved by the warming vacuum chamber. For reference, the cyclotron cooling rate $\Gamma \sim 1 \text{ s}^{-1}$ (at $B = 2 \text{ T}$) exceeds the expected buffer-gas cooling rate for nitrogen at pressures below 10^{-7} mbar .[?] In any case, it seems unlikely that such cooling would produce either so little or so uniform a change in the minimum plasma temperature as what was observed, over timescales where the pressure outside the trap varied by orders of magnitude.
- ³²C. Kurz, R. G. Greaves, and C. M. Surko, "Temperature dependence of positron annihilation rates in noble gases," *Phys. Rev. Lett.* **77**, 2929 (1996).
- ³³A. Hyatt, C. Driscoll, and J. Malmberg, "Measurement of the anisotropic temperature relaxation rate in a pure electron plasma," *Phys. Rev. Lett.* **59**, 2975 (1987).
- ³⁴C. Smorra, S. Sellner, M. J. Borchert, J. A. Harrington, T. Higuchi, H. Nagahama, T. Tanaka, A. Mooser, G. Schneider, M. Bohman *et al.*, "A parts-per-billion measurement of the antiproton magnetic moment," *Nature* **550**, 371–374 (2017).
- ³⁵B. d'Urso, B. Odom, and G. Gabrielse, "Feedback cooling of a one-electron oscillator," *Phys. Rev. Lett.* **90**, 043001 (2003).
- ³⁶C. J. Baker, W. Bertsche, A. Capra, C. L. Cesar, M. Charlton, A. C. Mathad, S. Eriksson, A. Evans, N. Evetts, S. Fabbri *et al.*, "Sympathetic cooling of positrons to cryogenic temperatures for antihydrogen production," *Nat. Commun.* **12**, 6139 (2021).
- ³⁷N. Evetts, P. Dosanjh, V. Zvyagintsev, and W. N. Hardy, "Note: A cryogenic, ultra-high-vacuum, microwave filter which passes a narrow beam," *Rev. Sci. Instrum.* **86**, 126101 (2015).
- ³⁸E. D. Hunter, "Cavity and microwave experiments on electron plasma," Ph.D. thesis (University of California, Berkeley, 2019).
- ³⁹C. Malbrunot, C. Amsler, S. Arguedas Cuendis, H. Breuker, P. Dupre, M. Fleck, H. Higaki, Y. Kanai, B. Kolbinger, N. Kuroda *et al.*, "The ASACUSA antihydrogen and hydrogen program: Results and prospects," *Philos. Trans. R. Soc. A* **376**, 20170273 (2018).
- ⁴⁰B. Radics, D. J. Murtagh, Y. Yamazaki, and F. Robicheaux, "Scaling behavior of the ground-state antihydrogen yield as a function of positron density and temperature from classical-trajectory Monte Carlo simulations," *Phys. Rev. A* **90**, 032704 (2014).
- ⁴¹F. Robicheaux, private communication (2022).
- ⁴²F. Peinetti, "Large-amplitude BGK modes in pure electron plasmas," Ph.D. thesis (Politecnico di Torino, 2005.).
- ⁴³J. Fajans, "Non-neutral plasma equilibria, trapping, separatrices, and separatrix crossing in magnetic mirrors," *Phys. Plasmas* **10**, 1209–1214 (2003).
- ⁴⁴Y. Enomoto, "Antihydrogen production in cusp trap," Ph.D. thesis (University of Tokyo, 2011).
- ⁴⁵M. Tajima, N. Kuroda, C. Amsler, H. Breuker, C. Evans, M. Fleck, A. Gligorova, H. Higaki, Y. Kanai, B. Kolbinger *et al.*, "Antiproton beams with low energy spread for antihydrogen production," *J. Instrum.* **14**, P05009 (2019).
- ⁴⁶J. Danielson, T. Weber, and C. Surko, "Extraction of small-diameter beams from single-component plasmas," *Appl. Phys. Lett.* **90**, 081503 (2007).